Texture, Strain, and Phase-Fraction Measurements during Mechanical Cycling in Superelastic NiTi

R. VAIDYANATHAN, M.A.M. BOURKE, and D.C. DUNAND

Superelastic NiTi was subjected to simultaneous neutron diffraction and uniaxial compressive cycling between 10 and 980 MPa. The objective was an *in-situ* investigation of the evolution of the stress-induced, reversible transformation between austenite and martensite, to determine the cause of the changes in the macroscopic stress-strain response with cycling. Rietveld refinement was used to analyze the neutron spectra and quantify the phase fraction, texture, and elastic strain. The average phase strain in the mechanically loaded austenite (at a given stress) remained unaltered during the 100 load-unload cycles. However, differences in both the volume fraction and texture of austenite and martensite were noted as cycling progressed, suggesting that these factors are responsible for the changes in the macroscopic stress-strain response of NiTi with mechanical cycling.

I. INTRODUCTION

SUPERELASTICITY is a deformation mechanism observed in NiTi and other allotropic, ordered alloys where the high-temperature cubic phase (austenite), when subjected to an external applied stress, transforms to a monoclinic phase (martensite), thus producing a macroscopic strain that augments the elastic strain. On removing the stress, the martensite is no longer stable and transforms back to austenite, resulting in a complete recovery of the macroscopic strain at the end of the mechanical cycle.[1,2] In various engineering applications,[3] superelastic alloys are subjected to repetitive loading and unloading accompanied by forward and reverse martensitic transformations of the parent austenite phase.

Previous studies[4–11] have documented changes in the stress-strain response of cyclically loaded superelastic NiTi. Some of the changes previously observed with an increasing number of cycles include an increase in the residual plastic strain in the unloaded state; a decrease in the stresses at which the martensitic transformation starts and finishes; a reduction in the load-unload stress hysteresis; and a decrease in the transformation strain range. Typically, the magnitude of these changes becomes smaller as the number of cycles increases, *i.e.*, the stress-strain curve tends toward a steady state for large numbers of cycles.

While theories have been proposed in previous investigations to explain these changes, no experimental studies examined the micromechanical and microstructural changes associated with the phase transformation (*e.g.*, volume fraction of martensite, internal strain fields, texture of the transformed martensite). Both neutron and X-ray diffraction, when performed under load, can be used to study these parameters in-situ during the transformation and to obtain phase-specific information. However, neutrons penetrate deeper than X-rays (several millimeters, compared to a few micrometers for X-rays from a conventional source). Thus, neutrons are uniquely suited to study the bulk behavior of polycrystalline samples without free-surface effects. This has been demonstrated in previous publications, where the phase fraction, texture, and strain evolution of mechanically loaded superelastic NiTi were characterized by *in-situ* neutron diffraction during a single mechanical cycle.[12,13]

In the present study, we report on the use of *in-situ* neutron diffraction during multiple compressive load-unload cycles to monitor the evolution of the stress-induced transformation in polycrystalline NiTi. As any initial texture is expected to significantly affect the properties of the transformation,[14] we used a polycrystalline sample with randomly oriented grains, unlike most of the previous studies cited earlier. Furthermore, we used compressive cycles, which have rarely been investigated but are known to differ from tensile cycles.[15]

II. EXPERIMENTAL PROCEDURES

Prealloyed NiTi powders (99.9 pct pure, 49.4 at. pct Ni, with a size between 44 and 177 μm, from Special Metals Corp., New Hartford, NY) were blended with Ni powders (99.9 pct pure, with a size between 44 and 177 μm, from Special Metals Corp.). The powders (with a nominal average composition of 51.0 at. pct Ni) were packed in a low-carbon steel container (thickness of 0.318 cm, i.d. of 2.5 cm, and length of 12 cm, lined with a boron-nitride-coated nickel foil to prevent carbon contamination) and were subjected to hot isostatic pressing (HIP) at 1065 °C and 100 MPa for 3 hours. A cylindrical specimen 8 mm in diameter and 20 mm in length was electro-discharge machined from the resulting billet. This sample was solutionized at 1000 °C for 1 hour and oil-quenched to room temperature in titanium-gettered flowing argon, annealed at 400 °C for 1 hour in air, and quenched in ice water.

Neutron diffraction measurements were performed in "time-of-flight" mode using the neutron powder diffractometer at the pulsed neutron source at Los Alamos National

R. VAIDYANATHAN, formerly Postdoctoral Associate, Laboratory for Experimental and Computational Micromechanics, Massachusetts Institute of Technology, is Assistant Professor with the Advanced Materials Processing and Analysis Center (AMPAC) and the Mechanical, Materials and Aerospace Engineering Department at the University of Central Florida, Orlando, FL 32816. M.A.M. BOURKE, Technical Staff Member, is with LANSCE/MST-8, Los Alamos National Laboratory, Los Alamos, NM 87545. D.C. DUNAND, Associate Professor, is with the Department of Materials Science and Engineering, Northwestern University, Evanston, IL 60208.

Manuscript submitted May 1, 2000.

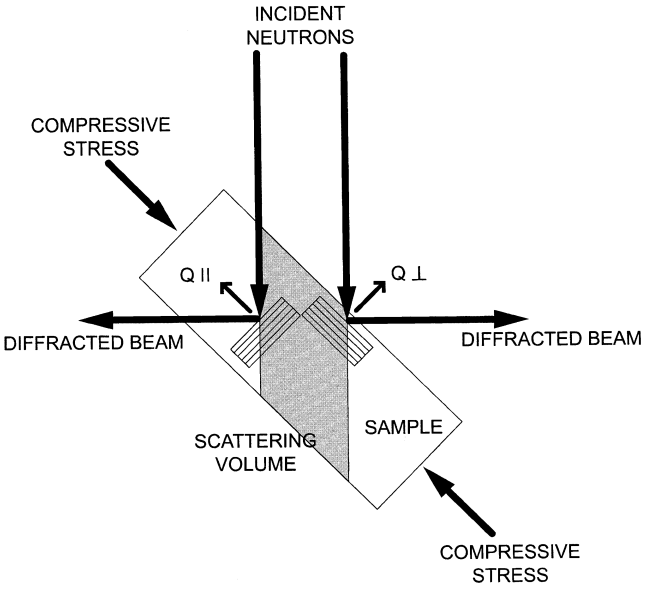

Fig. 1—A schematic of the experimental setup at Los Alamos National Laboratory showing the scattering vectors (**Q**) and their relationship with the loading axis. The irradiated volume is about 1 cm^3.

Table I. Stresses, Cycle Numbers, and Designations at Which Neutron Spectra Were Obtained during Mechanical Cycling of Superelastic NiTi

Cycle number	Cycle designation	Stress (MPa)
1	C1	−8
1	C1	−715
1	C1	−988
1	C1	−544
2	C2	−8
2	C2	−715
2	C2	−988
2	C2	−544
3	C3	−8
101	C101	−8
101	C101	−715
101	C101	−988
101	C101	−544
102	C102	−8

Laboratory (LANL). Detailed information on the experimental setup can be found elsewhere[16,17] and is only summarized here. The sample was mechanically loaded in uniaxial compression while neutron diffraction spectra were simultaneously acquired in three scattering geometries. The loading axis formed an angle of 45 deg to the incident neutron beam, allowing measurements in opposing 90 deg detectors, for which the scattering vectors were parallel and perpendicular to the loading axis. A schematic of the experimental setup showing the scattering vectors (**Q**) and their relationship with the loading axis is shown in Figure 1. A third detector was used in a back-scattering geometry, for which the scattering vector was 61 deg from the loading axis (not shown in the figure).

A total of 101 load-unload compressive cycles were completed at ambient temperature, each between −8 to −988 MPa, with diffraction data obtained at various applied stresses during selected cycles. The stresses and respective cycle numbers at which neutron data were obtained are summarized in Table I. For intermediate cycles where no neutron data were collected, the crosshead displacement rate was ±3 mm/min (corresponding to a full cycle of about 40 seconds), while for neutron diffraction cycles, it was 30 times slower. Average sample temperature changes of about 10 °C to 14 °C due to transformation enthalpy dissipation were recorded during the fast cycles. For the slower cycles during neutron data acquisition, no measurable changes in temperature were noted.

Due to constraints in the enclosed testing chamber used for neutron diffraction, an extensometer could not record macroscopic stress-strain data during the *in-situ* mechanical tests. Hence, the same sample first used in the *in-situ* test was subsequently heat-treated, as described previously, and subjected to *ex-situ* mechanical testing. The heat treatment removed any microstructural changes that occurred during the *in-situ* cycling, and the use of a single sample eliminated uncertainties associated with the introduction of a second sample (*e.g.* minute composition variations that can have a large effect on the stress-strain behavior of NiTi[1]). During the *ex-situ* tests, an extensometer was attached to the sample and the same cycling procedure described previously was followed. Furthermore, a compression cage was used to ensure that there was no misalignment during compression testing. Given the identical initial composition and heat treatment, as well as the high solutionizing temperature and titanium-gettered flowing argon atmosphere, we assume that data from the two tests are identical and do not distinguish between them in the present article.

Previous observation by optical microscopy[18] showed the sample to be pore-free, with an average austenitic grain size of 20 μm. Density measurements by water displacement gave a density within 0.2 pct of the theoretical value. Differential scanning calorimetry with a PERKIN-ELMER* DSC-7 calorimeter at a rate of 1 K-min^{-1} under nitrogen cover gas was used to investigate the martensite start and finish temperatures. Temperatures as low as −140 °C were approached with no observable transformation. The observation that the martensite can be stress induced but not temperature induced has been discussed previously.[19]

*PERKIN-ELMER is a trademark of Perkin-Elmer Physical Electronics, Eden Prairie, MN.

III. NEUTRON DIFFRACTION DATA ANALYSIS

We have previously established a methodology[12] to analyze neutron diffraction data from stress-induced transformations in NiTi and applied it to superelastic NiTi and NiTi composites deformed during a single cycle.[19,20] This methodology is summarized subsequently, with emphasis placed on observing changes in the stress-induced austenite-martensite transformation on cycling.

The Rietveld refinement[21] technique, implemented in the LANL code General Structure Analysis System (GSAS),[22] is used to analyze the neutron diffraction spectra. In the Rietveld method, the intensity at every point in the spectrum is determined by adding the calculated background and Bragg scattering intensities corresponding to diffraction peaks. The refinement procedure varies selected parameters (*e.g.*, phase volume fractions, atom positions, and phase texture) until the calculated and measured spectra match in

a least-squares fit. Errors are quantified and are associated with the statistics of the fit. In particular, the procedure incorporates changes in diffraction-peak intensities due to texture. A generalized spherical harmonic description[23,24] is used to account for the evolving texture in the austenite and martensite phases. The profile function that fitted the data best is a combination of two functions: the first is the result of convoluting two back-to-back exponentials with a Gaussian function, and the other is a linear combination of a Lorentzian and a Gaussian (pseudo-Voigt) function.

For the austenite, two formulations of the elastic strain are used. In the first approach, the refinement incorporates no description of any strain anisotropy, and the strain is determined from lattice parameters obtained as best fits. The elastic lattice strain in the austenite, for a given compressive stress (S) and cycle (C), is then reported as

$$\varepsilon_S^C = \frac{a_S^C - a_0^1}{a_0^1} \qquad [1]$$

where a_S^C is the austenite lattice parameter at the applied compressive stress during the cycle, and a_0^1 is the lattice parameter under no external load at the start of the first cycle, *i.e.*, the untested sample. A nominal compressive stress of −8 MPa was used to hold the sample horizontally in the stress rig and corresponds to this "zero-stress" condition.

In the second approach, a strain-anisotropy term is incorporated in the Rietveld procedure, and the strain is reported for a specific crystallographic plane as a contribution of isotropic (*hkl*-independent) and anisotropic (*hkl*-dependent) components. The isotropic strain component is determined by shifting individual diffraction peaks so as to account for a change in the lattice parameter, as in Eq. [1]. The anisotropic strain component further shifts individual peaks proportionate to $(h^2k^2 + h^2l^2 + k^2l^2)/(h^2 + k^2 + l^2)^2$, where (*hkl*) is the plane-specific reflection.[12]

Martensitic diffraction peaks were not characterized for strain evolution, since the lattice-parameter value for the nascent, unloaded martensite cannot be easily determined. In addition, the large number of broad overlapping reflections due to the low symmetry and small size scale of the monoclinic martensite make it difficult for the Rietveld refinement to converge while strains are physically described in the martensite. Rather, the emphasis for the martensite was to accurately characterize the volume fraction and texture.

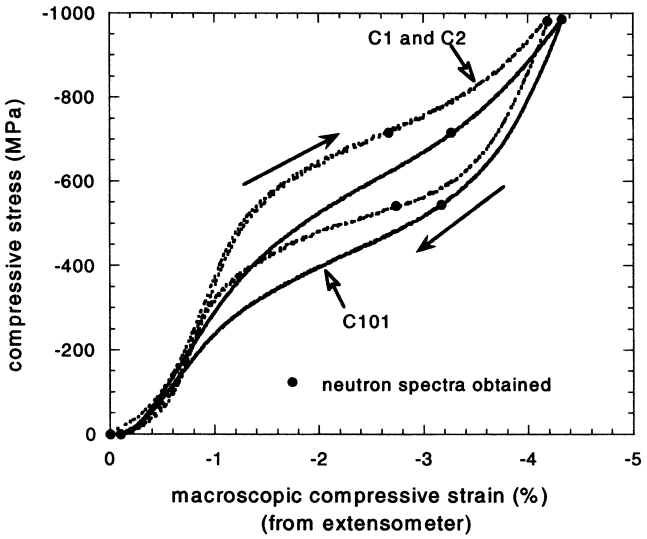

Fig. 2—Macroscopic stress-strain response of superelastic NiTi (from extensometer) for cycles C1, C2, and C101, showing stresses at which loading was interrupted and neutron spectra recorded. The ramp rate during the cycles was 0.1 mm/min.

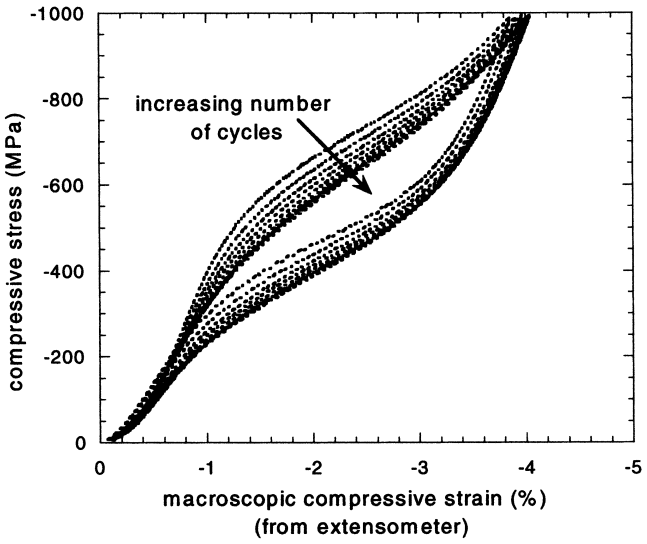

Fig. 3—Macroscopic stress-strain response of superelastic NiTi (from extensometer) for cycles C10, C20, C30, C40, C50, C60, C70, C80, C90, and C100. The ramp rate during the cycles was 3 mm/min.

IV. RESULTS

Macroscopic stress-strain curves corresponding to the three mechanical cycles (C1, C2, and C101) for which neutron diffraction spectra were acquired are shown in Figure 2. The loading half of the curve consists of an initial region where austenite deforms elastically up to about 300 MPa, a subsequent broad region where stress-induced martensite is formed up to about 800 MPa, followed by a final region where elastic deformation of the martensite is dominant. On unloading, the same three regions are observed in the opposite order. The evolution with cycling of the macroscopic stress-strain loops can be seen in Figure 3, where loops at intervals of ten cycles are superimposed on the same graph. The following systematic changes in the macroscopic stress-strain curves in Figures 2 and 3 are observed with increased cycling:

(1) the stresses at which the martensitic transformation initiates and finishes decrease;
(2) the mechanical hysteresis (*i.e.*, the area between the loading and unloading curves) becomes smaller;
(3) the transformation strain measured at the maximum stress increases (this increase is larger than any possible nonrecoverable strain accumulation); and
(4) the rate of the aforementioned changes decreases.

Furthermore, the following two observations specifically address the initial cycles:

(5) A nonrecoverable compressive residual strain of 0.1 pct was recorded at the end of the first cycle, but no significant nonrecoverable strains were observed upon subsequent cycling.

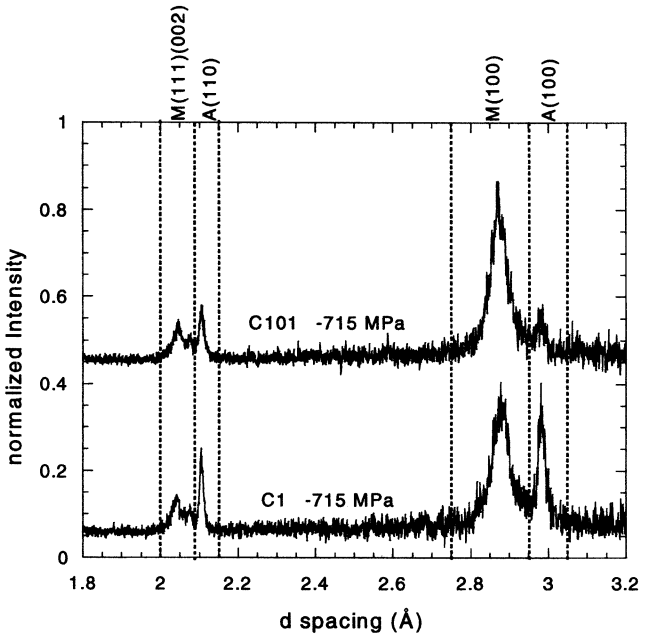

Fig. 4—Neutron diffraction spectra from NiTi at −715 MPa (during loading) for cycles C1 and C101. The peaks shown here are from lattice planes perpendicular to the applied stress.

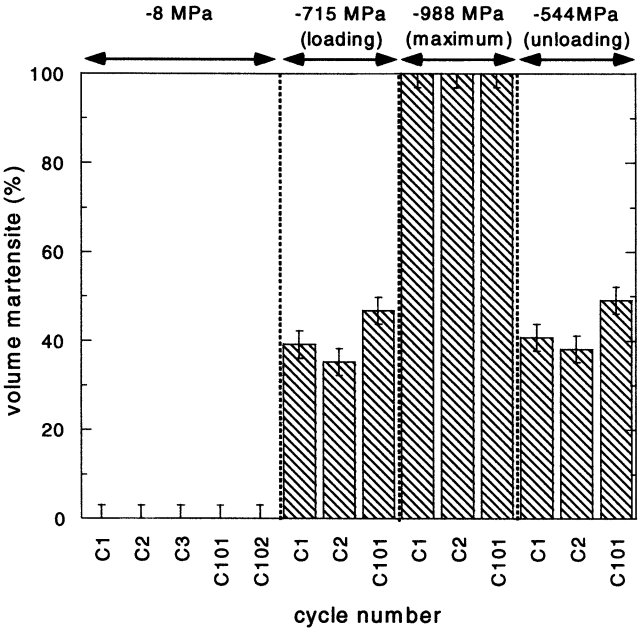

Fig. 5—Volume martensite (pct) at various stresses for the different cycles.

(6) NiTi is expected to be austenitic at stresses below 300 MPa, and, hence, a linear stress-strain response is predicted due to the elastic deformation of the austenite. However, the first few cycles showed some nonlinearity even at these low stresses, when compared to later cycles. Owing to the use of a compression cage and extensometer, these nonlinearities are believed to be material-specific and not related to misalignment of the testing fixtures.

Here, we note that Figures 2 and 3 cannot be directly compared, since the stress-temperature equivalence, as given by the Clausius–Clapeyron equation, can be between 3.3 and 13 MPa/K.[25] Consequently, temperature differences of 10 °C to 14 °C due to faster cycling would alter the stress at which the transformation initiates and completes. Additionally, it may be argued that differences between the *in-situ* and *ex-situ* samples exist as a result of the additional thermal treatment. The motivation for including the well-known trends[4–11] illustrated in Figure 3 is merely for completeness, as it confirms the stress-strain curve evolution occurring between cycles C2 and C101, shown in Figure 2. No quantitative data were obtained corresponding to the intermediate cycles from the *ex-situ* sample.

Excerpts of diffraction spectra corresponding to cycles C1 and C101, both at −715 MPa (during loading), are shown in Figure 4. Differences in relative peak intensities are observed between cycles C1 and C101, which, given the depth of penetrations of neutrons, can be attributed to changes occurring in the bulk volume of the sample. Figure 5 shows the martensite volume fraction as obtained by Rietveld refinement for the stresses and cycles in which neutron spectra were acquired (marked in Figure 2).

The texture in the austenite and martensite, obtained by using a spherical harmonic description in the Rietveld refinement, is presented in two ways. The first utilizes the texture index J, which represents the magnitude of the texture by a single number. This number is obtained by integrating over all space the orientation distribution function (a function which maps the probability of each of the possible grain orientation with respect to the external sample dimensions).[24,26] The texture index varies between unity and infinity (corresponding to a polycrystal with a random orientation and ideal single crystals, respectively). The second texture presentation uses axial distribution plots which correspond to a radial slice through the pole figure and are applicable here because of the cylindrical symmetry in the sample. In an axial distribution plot, the *y*-axis is a measure of the number of grains (relative to a randomly oriented polycrystal) that are oriented at an angle (ϕ) between that normal to the plane under consideration and a chosen axis in the specimen, in this case the loading axis. Thus, the axial distribution plot for a random polycrystalline sample would be represented by a horizontal line at unity. Given the variable volume fractions and crystallographic symmetries (*i.e.*, cubic austenite and monoclinic martensite), texture indices or axial distribution plots cannot be compared between phases but are limited to relative changes for the same phase.

Figures 6 and 7 present the texture index of austenite and martensite, respectively, at the stresses and cycle numbers at which neutron spectra were obtained. From these figures, the following observations can be made.

(1) There is no significant texture developed in the austenite at the no-load condition after cycling. This is evident from a value of unity for the unloaded austenite in cycles C101 and C102 at −8 MPa, shown in Figure 6.
(2) At intermediate stresses the austenite exhibits a texture that increases with cycling (Figure 6). This is evident from a value of $J = 1.10$ at −715 MPa during loading for cycles C1 and C2, increasing to $J = 1.40$ for cycle C101. Similarly, the texture index of austenite has a value of $J = 1.06$ at −544 MPa during unloading for cycles C1 and C2, increasing to $J = 1.33$ for cycle C101.

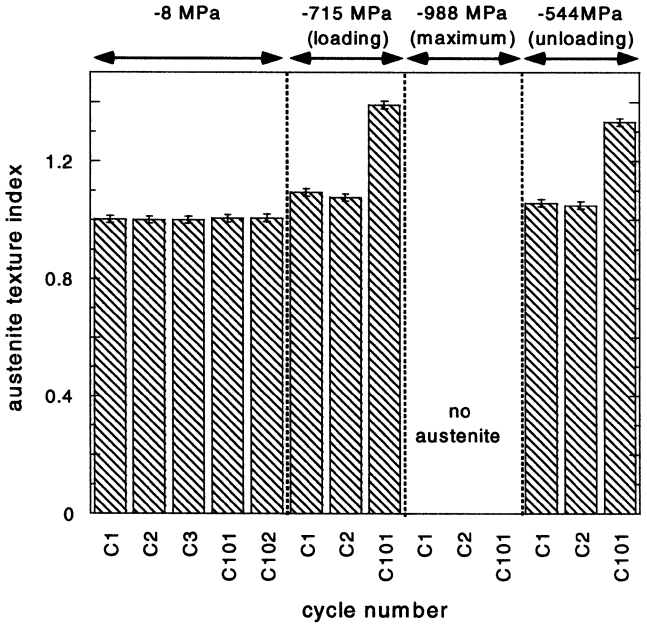

Fig. 6—Austenite texture index at various stresses for the different cycles.

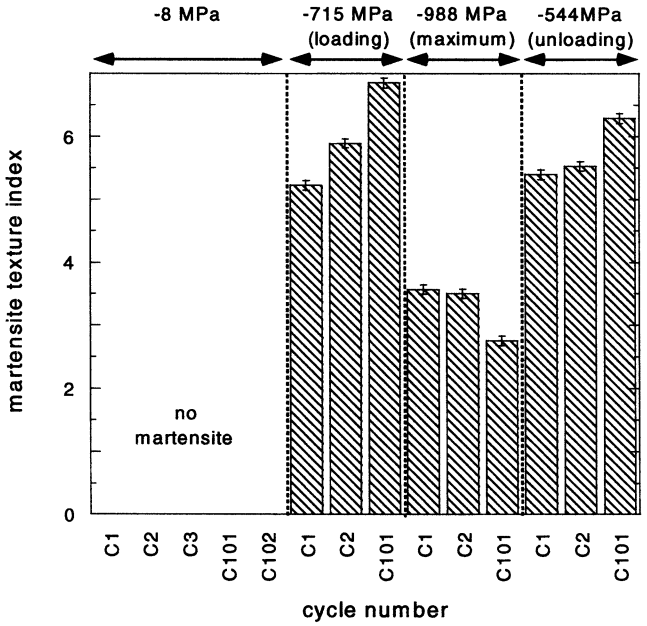

Fig. 7—Martensite texture index at various stresses for the different cycles.

(3) At a given stress, the martensite texture changes noticeably between cycles C2 and C101, with a decrease at the maximum stress (−988 MPa) and an increase at intermediate stresses during loading and unloading.

Figures 8 through 13 are axial distribution plots for the cycles in which neutron spectra were acquired, supplementing the information provided by the texture index in Figures 6 and 7. In these figures, the horizontal line at unity corresponds to a random polycrystal, as described previously. Figure 8 shows the (100) axial distribution plot for austenite in the unloaded condition, which is very close to unity. Figure 8, thus, does not show any development of

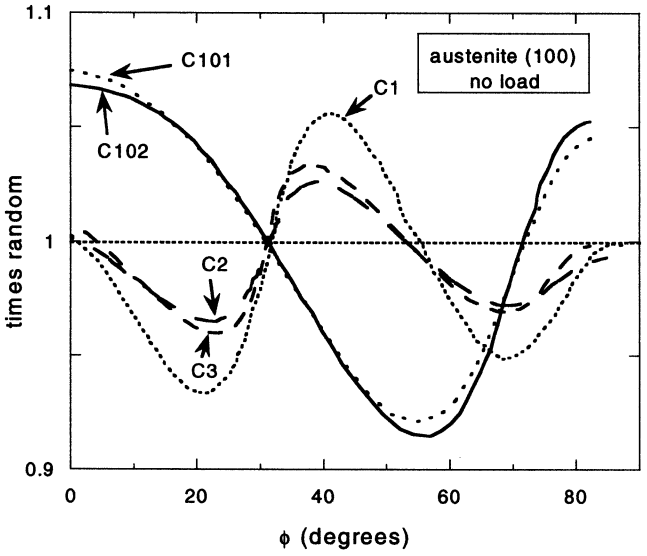

Fig. 8—(100) axial distribution plot for austenite in the no load condition at the start of cycles C1, C2, C3, C101, and C102.

texture in the orientation of (100) austenite planes in the unloaded state. The scatter in the axial distribution plots can be attributed to fluctuations in the orientation distribution function. Figures 9(a) and (b) show the (100) axial distribution plots for austenite in the loaded condition at −715 MPa (during the loading part of the cycle) and at −544 MPa (during the unloading part of the cycle), respectively. These two stresses, which are unequal because of the mechanical hysteresis between the forward and reverse transformations, were selected to give a balanced austenite-martensite volume fraction (about 40 vol. pct of austenite (Figure 5) during the loading and unloading parts of the cycle). Figures 9(a) and (b) show the (100) austenite planes becoming significantly more textured at the intermediate loads (−715 and −544 MPa, respectively) with cycling. For our scattering geometry, the shape of the curves in Figures 9(a) and (b) correspond to the preferential disappearance of (100) austenite planes aligned perpendicular and parallel to the loading direction. The removal of these planes results in a larger fraction of austenite (100) planes that are oriented 45 deg to the loading direction, as evidenced by a peak around $\phi = 45$ deg.

Figure 10 shows the (100) axial distribution plot for the fully transformed martensite at maximum stress (−988 MPa), while Figures 11(a) and (b) correspond to the partially transformed condition (−715 and −544 MPa during the loading and unloading parts of the cycle, respectively). In these figures, there is no physical significance associated with values of less than zero, which are an artifact of the global normalization procedure. In order to illustrate texture for other crystallographic directions and investigate the type of twinned structure prevalent, Figure 12 presents the axial distribution plot for (0-1 1) in martensite, and Figure 13 presents that for (111) in austenite, from cycle C1 at −715 MPa during loading.

Figure 14 shows the elastic lattice strains (Eq. [1]) in the austenite at the various stresses for the different cycles. Figure 15 present the same data as in Figure 14 but, as

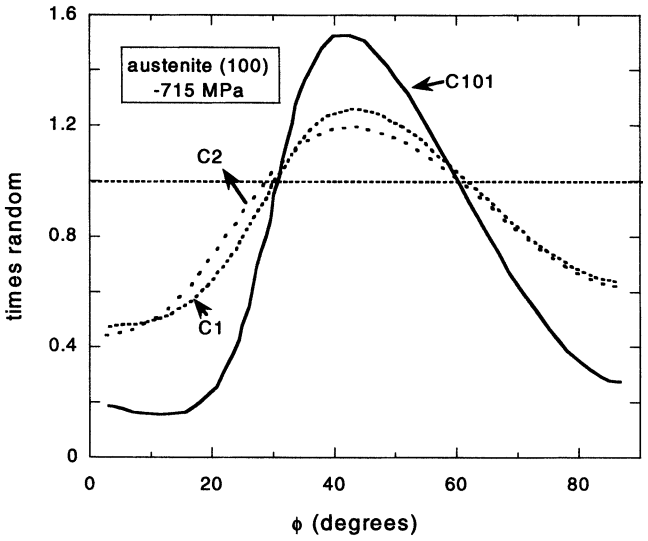

(*a*)

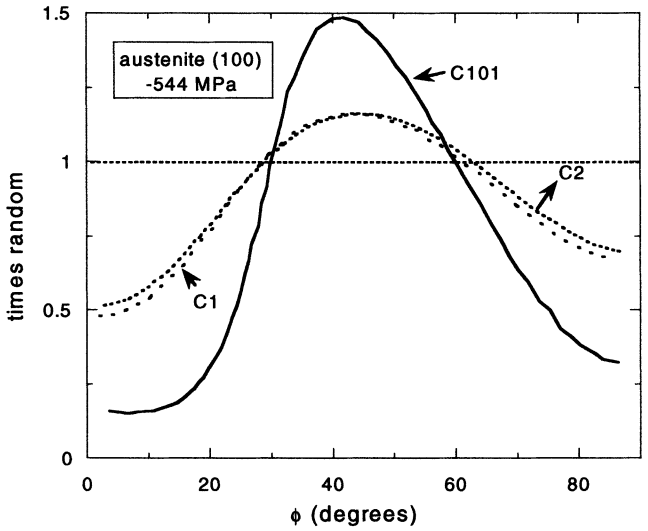

(*b*)

Fig. 9—(100) axial distribution plot for austenite from cycles C1, C2, and C101 during (*a*) the loading part of the cycle at −715 MPa and (*b*) the unloading part of the cycle at −544 MPa.

described previously, deconvolutes the strain into an isotropic component (which is lattice-plane independent) and an anisotropic component (which is lattice-plane dependent).

V. DISCUSSION

The measured evolution of the macroscopic stress-strain curves in Figure 3 and previously reported work[5–9] both indicate that 100 cycles are sufficient to achieve almost-complete stabilization of the transformation in our sample. Furthermore, in previous work,[12,13,19] we consistently observe that most of the evolution occurred in the first few cycles, as illustrated by the nonrecoverable compressive residual strain of 0.1 pct occurring only after the first cycle. This evolution during the initial cycles is the reason why certain superelastic devices are "trained" through mechanical cycles before being utilized in their engineering applications.[2,6]

In the following sections, the observed changes in the

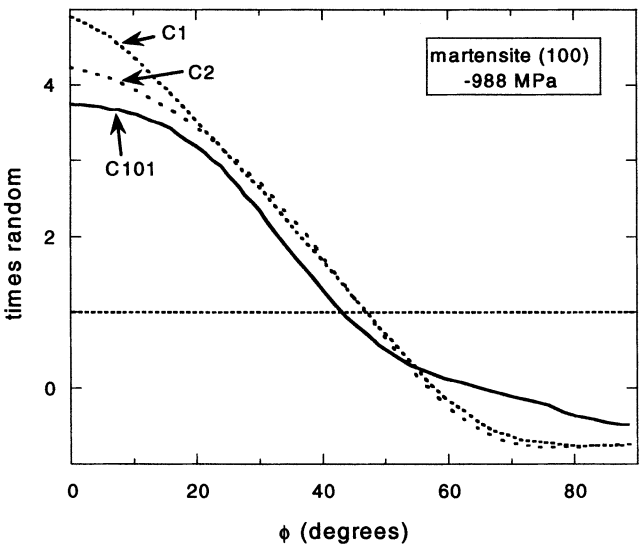

Fig. 10—(100) axial distribution plot for martensite at −988 MPa for cycles C1, C2, and C101.

macroscopic stress-strain curves are discussed in the light of the evolution of microstructural phase texture and volume fraction and micromechanical elastic strains, as obtained from *in-situ* neutron diffraction.

A. *Volume-Fraction Evolution with Cycling*

In our previous work on similar NiTi samples subjected to a single mechanical cycle,[19] we observed a linear relationship between the volume fraction of martensite present in the diffraction volume (about 1 cm^3) and the macroscopic sample superelastic strain. The superelastic strain is defined as the total strain measured by extensometry from which the elastic strain has been subtracted. In that work, since no significant load transfer/partitioning was observed between the austenite and martensite phases (*i.e.*, the applied stress *vs* phase-strain response was mostly linear), no distinction was made between the austenite and martensite elastic moduli in determining the superelastic strain; a value of 51 GPa was used for the elastic modulus of NiTi. The fact that about 40 vol pct of martensite existed at the two intermediate stresses during loading and unloading confirms that the transformation occurs uniformly in the bulk and that deformation is homogeneous. This contrasts with the highly localized deformation processes operating by growth of Luders bands observed in some superelastic NiTi samples deformed in tension.[27]

From the linear slope of the martensite volume fraction *vs* superelastic strain response described previously, about 40 vol pct martensite resulted in 1 pct superelastic strain. From Figure 2, there is a 0.006 increase in superelastic strain between cycles C101 and C1, at −715 MPa during loading. The corresponding increase at −544 MPa during unloading is 0.004. If this increase in superelastic strain were to be solely caused by a change in the volume fraction of martensite, the corresponding increase in the volume fraction of martensite would be 24 and 16 pct, respectively. However, Figure 5 shows that the increase in the martensite volume fraction is less than the aforementioned values but is statistically significant. It can then be concluded that two mechanisms are responsible for the evolution of the stress-strain

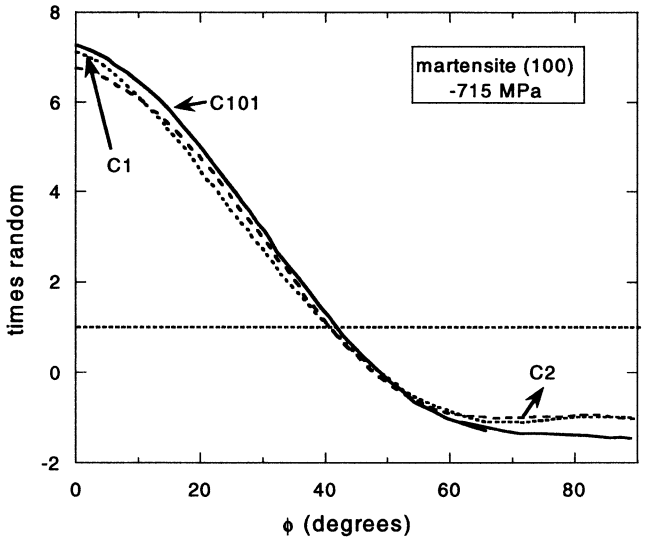

(*a*)

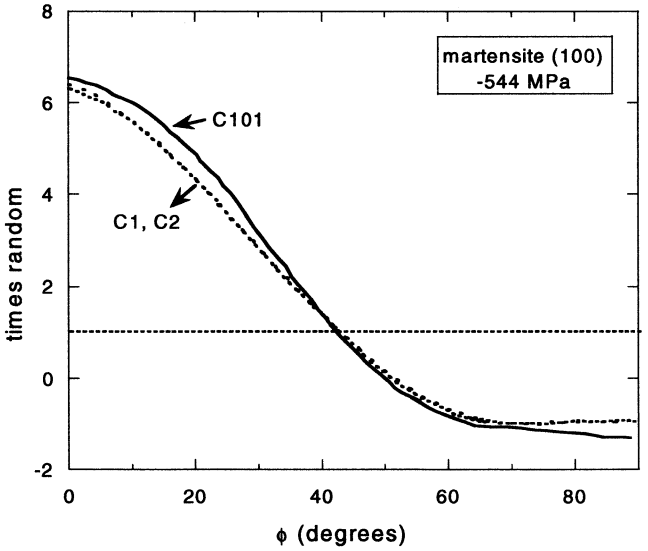

(*b*)

Fig. 11—(100) axial distribution plot for martensite from cycles C1, C2, and C101 during (*a*) the loading part of the cycle at −715 MPa and (*b*) the unloading part of the cycle at −544 MPa.

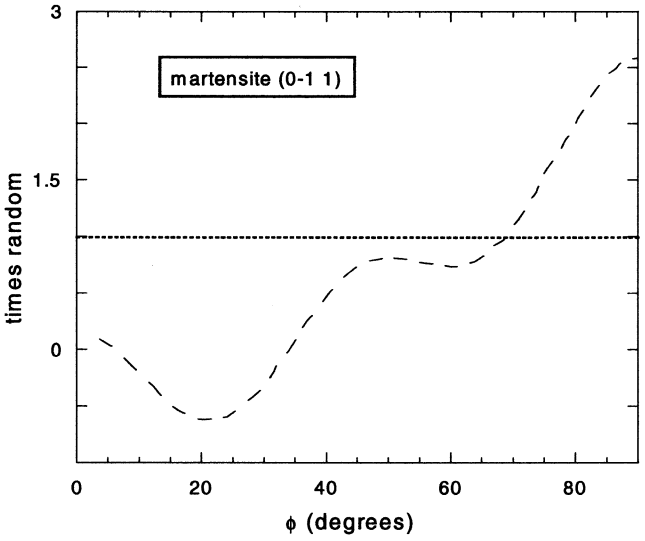

Fig. 12—Axial distribution plot for (0–11) martensite from cycle C1 at −715 MPa during loading.

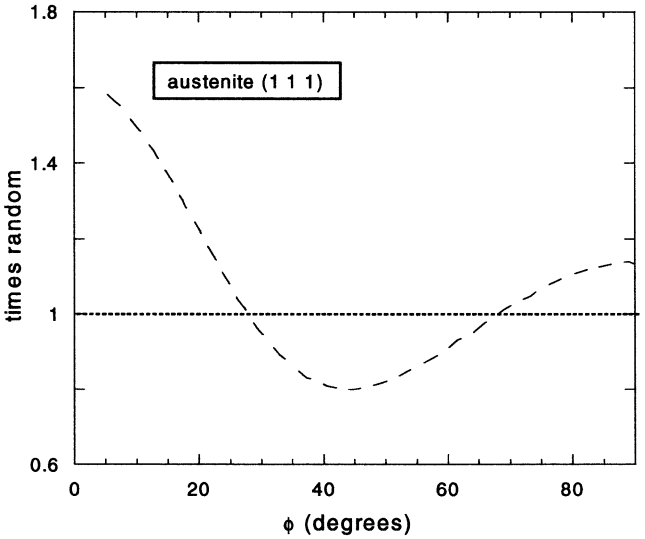

Fig. 13—Axial distribution plot for (111) austenite from cycle C1 at −715 MPa during loading.

curve during mechanical cycling at intermediate stresses (while martensite and austenite coexist): first, more martensite is formed at a given stress; and second, the same volume fraction of martensite generates somewhat larger uniaxial strains. The second effect is discussed in Section B in terms of texture.

At the peak stress in Figure 2, the difference in strain between cycles C101 and C1 is about 0.0015 corresponding to 6 vol pct martensite. However, Figure 5 shows that the volume fraction of martensite is unity in both cases, within the experimental sensitivity of neutron diffraction of about 3 vol pct (*e.g.*, some retained austenite in the initial cycles). This, again, indicates that a given amount of martensite produces more strain after mechanical cycling. Similarly, in the unloaded state, it is possible that a small volume fraction of martensite may be responsible for the nonrecoverable compressive residual strain of 0.1 pct, which was only recorded after the first training cycle. Finally, small volumes of austenite transforming to martensite can also justify the nonlinearity in the initial elastic range of the macroscopic stress-strain response in the earlier cycles (Figure 2). Differences between neutron diffraction and extensometer determinations of the moduli were attributed to these small volume fractions in our earlier work.[19,20] This hypothesis is further substantiated in light of the changes in the texture and strain fields, as discussed in Sections B and C.

B. *Texture Evolution with Cycling*

The fact that the austenite does not exhibit texture in the unloaded, as–heat-treated state (start of cycle C1) is expected, since the samples were fabricated by HIP of randomly oriented powders. The evolving texture in the austenite at higher loads can be attributed to the crystallography of the martensitic transformation. The unique lattice correspondence existing between austenite and martensite[28] and

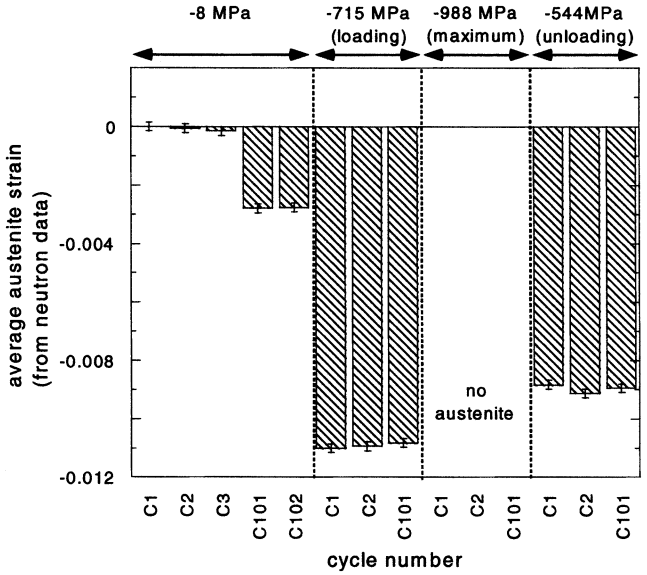

Fig. 14—Average strain in austenite from diffraction data (Eq. [1]) at various stresses for the different cycles.

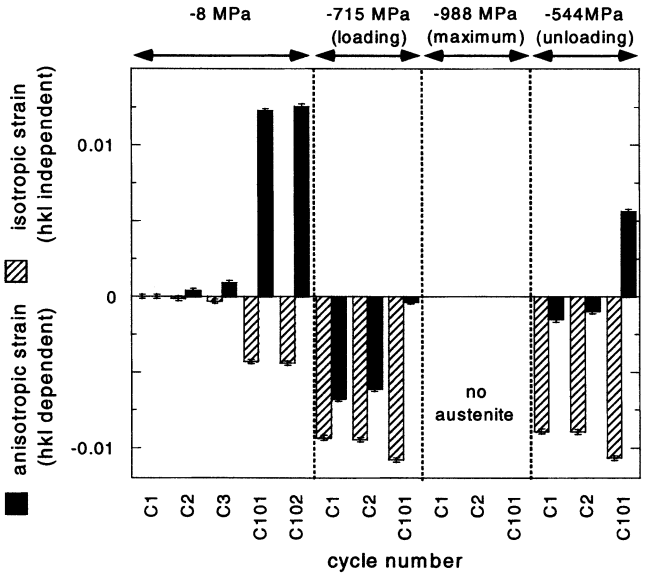

Fig. 15—Anisotropic and isotropic components of the average strain in austenite at various stresses for the different cycles.

the formation of highly textured martensite results in austenite developing texture as well. This is analogous to developing texture by removing grains with a given crystallographic orientation in an originally untextured sample. This mechanism of texture evolution in austenitic NiTi has been previously suggested.[12,13]

Stress-induced martensite forming from untextured austenite is expected to be textured, as variants that give a large macroscopic strain in the direction of the applied stress and whose transformation strain can be accommodated are expected to preferentially form. The macroscopic uniaxial superelastic strain that is generated on application of stress as austenite transforms to martensite can originate from (1) the transformation of austenite to martensite or (2) twinning of previously transformed martensite. However, on comparing the variants that were preferentially formed by twinning during uniaxial compressive loading of NiTi consisting of thermally induced martensite, we found that the nascent stress-induced martensite has a (1 1 −1) type I twinned structure.[29] In the case of thermally induced martensite subjected to loading, the orientation observed can be predicted on the basis of strains calculated as one variant transforms to a more favorable one.[28,30] The general shape of the axial distribution plots in Figures 10, 11(a), and 11(b) correspond to (100) martensite planes aligning perpendicular to the loading direction. This was also qualitatively observed, as the (100) martensite peak was present in one detector but absent in the other. This alignment of (100) martensite planes, along with the alignment of (0 −1 1) martensite planes parallel to the loading direction in Figure 12, is consistent with a (1 1 −1) type I twinned structure. This has been previously observed in neutron diffraction spectra.[29] However, in that earlier work, only single peaks in the spectra were used to qualitatively follow the intensity, and a more comprehensive Rietveld analysis was not used. The correspondence between austenite and martensite can be used to justify the preferential disappearance of (100) austenite parallel and perpendicular to the loading direction (Figures 9(a) and (b)). Similarly, a larger fraction of (111) austenite planes align perpendicular to the loading axis (Figure 13). The (1 1 −1) type I twinned orientation of the stress-induced martensite was confirmed by examining other lattice planes and is not discussed in detail here to avoid redundancy.

Given that the cycling-induced increase in the martensite volume fraction formed at the same applied stress (Figure 5) can account for only part of the cycling-induced increase in macroscopic strain in Figure 2, it is not surprising that the texture increases as well with cycling (Figure 7). The physical reasons for these changes in texture are, however, not clear. One possible reason is that residual mismatch strains initially present in the material after heat treatment become progressively relaxed as cycling progresses, thus allowing for a different, more efficient transformation path in stress-strain space. Another possible explanation is based on the minimization of the mismatch between the transformed martensite and the transforming austenite. This mismatch can be elastic (due to differences in the elastic modulus between austenite and martensite) and/or allotropic (due to differences in the volume and shape between austenite and martensite). Consequently, the local internal stress field associated with grain boundaries and interfaces is altered so as to minimize the hysteresis and associated interface friction. This alteration may result in martensite initially forming at lower stresses or more-favorable orientations of martensite forming at lower stresses. This is consistent with a reduction in the mechanical hysteresis and a lowering of the stress at which the transformation apparently starts (and finishes), as observed in Figure 3. The source of changes in the internal stress field could also be dislocations that are associated with slip and nonrecoverable strains (*e.g.*, the 0.1 pct nonrecoverable plastic strain observed between the first and second cycles in Figure 2), as proposed by Melton and Mercier.[4] Another possibility is the formation of a martensite that is stabilized in the presence of internal stresses and exists even at low or no external applied stresses. Such a martensite may explain the nonlinearity in the initial portion of the stress-strain curve described previously and the

observed changes in the martensite texture index between cycles C1 and C2 at intermediate loads, shown in Figure 7.

Changes with cycling in the axial distribution plots in Figures 11(a) and (b) are not as significant as those of the texture index in Figure 7. This is at first surprising, but can be understood by considering that the texture index is an overall integrated measure indicating the degree of alignment of all the diffracting crystals (obtained by integrating the orientation distribution function over all space), while the axial distribution plots present orientation information for specific planes. Consistent with Figure 7, Figure 10 shows (100) martensite planes decreasing in texture at −988 MPa with cycling. This decrease in the texture of martensite at maximum load with cycling may be due to the fact that austenite grains in favorable orientations with respect to the applied stress transform prior to grains in less favorable orientations. The grains that transform as the transformation progresses are subject to greater constraints (stress, strain, and thermodynamic compatibility) and, hence, cannot form to merely maximize the transformation strain. Thus, as the texture at intermediate stresses increases with cycling (as described previously), the final texture at −988 MPa (as seen in Figures 7 and 10) decreases with cycling.

C. *Elastic-Strain Evolution with Cycling*

The average elastic strain in austenite (as measured from Eq. [1]) does not change at intermediate loads on cycling (Figure 14), even though more martensite exists for the same applied stress (Figure 5). This suggests that stress-induced martensite very efficiently accommodates the large allotropic mismatch with the untransformed austenite. A similar mismatch accommodation has been previously observed in superelastic NiTi and NiTi-TiC composites.[19,20]

However, the average residual elastic strain in the austenite changes for the unloaded state with cycling, as shown in Figure 14 (−0.00276 for cycle C101). Furthermore, from Figure 15, it is seen that the anisotropic and isotropic components of the strains change and redistribute themselves on cycling. Both these observations could arise due to

(1) changes in the texture of the austenite;
(2) dislocation slip associated with the macroscopic nonrecoverable plastic strain (as proposed previously[4]);
(3) the strain redistribution alluded to previously, which may not be due to slip; or
(4) martensite that is formed and stabilized due to internal stresses and/or slip, as described previously.

Since the austenite in the no-load condition in cycles C101 and C102 shows no significant texture (Figures 6 and 8), it is unlikely that effect 1 dominates, because changes in the isotropic and anisotropic components of the strain in austenite are also observed at these no-load conditions. The changes in the isotropic and anisotropic components of strain on plastic deformation due to strain redistribution have been previously reported for steel,[31] substantiating effects 2 and 3. Effect 4, *i.e.*, residual martensite, can be expected to have a similar effect. While the exact reason for the redistribution of the anisotropic and isotropic components is not known, the result presented here is a direct observation of the expected changes in the internal stress field with cycling.[2]

VI. CONCLUSIONS

While the evolution during mechanical cycling of the macroscopic stress-strain loop of superelastic NiTi has been previously studied,[4–9] we present here for the first time a systematic study of the microstructural and micromechanical changes responsible for this evolution, using *in-situ* neutron diffraction measurements.

1. The change in macroscopic stress-strain behavior at intermediate stresses, where martensite and austenite coexist, is due to an increase in both the volume fraction and texture in the stress-induced martensite.
2. The average elastic strain in the austenite remains mostly unchanged at intermediate stresses, but the isotropic and anisotropic components of the strain in the austenite redistribute themselves. The residual elastic strain present after unloading in the austenite evolves during cycling.

While a quantitative explanation for these changes is beyond the scope of this article, these phenomenological observations shed light on the materials evolution occurring during repeated reversible stress-induced transformation in superelastic NiTi, of importance both during mechanical training of NiTi devices and during their subsequent use. The direct observation that texture evolution plays an important role during cycling suggests that different initial textures could significantly change the stress-cycling response of superelastic alloys. This could be adapted in engineering applications of superelastic materials, reducing the number of training cycles needed or increasing the total fatigue life[32] of such materials.

ACKNOWLEDGMENTS

The Manuel Lujan Jr. Neutron Scattering Center is a national user facility funded by the United States Department of Energy, Office of Basic Energy Science and Defense Programs. This work was supported, in part, by DOE Contract No. W-7405-ENG-36. RV and DCD acknowledge the support of Daimler-Benz (Daimler-Chrysler) AG, Stuttgart, Germany) in the form of a research grant and RV's participation in the MIT-Germany program. The authors also thank Dr. M.R. Daymond (LANSCE/Rutherford Appleton Laboratory) and Mark Seniw (NWU) for valuable experimental help.

REFERENCES

1. *Shape Memory Alloys*, H. Funakubo, ed, Gordon and Breach, New York, NY, 1987.
2. *Engineering Aspects of Shape Memory Alloys*, T.W. Duerig, K.N. Melton, D. Stoeckel, and C.M. Wayman, eds., Butterworth-Heinemann, London, 1990.
3. *Shape Memory Materials*, K. Otsuka and C.M. Wayman, eds., Cambridge University Press, Cambridge, United Kingdom, 1998.
4. K.N. Melton and O. Mercier: *Acta Metall.*, 1979, vol. 27 , pp. 137-44.
5. S. Miyazaki, T. Imai, K. Otsuka, and Y. Suzuki: *Scripta Metall.*, 1981, vol. 15, pp. 853-56.
6. S. Miyazaki, T. Imai, Y. Igo, and K. Otsuka: *Metall. Trans. A*, 1986, vol. 17A, pp. 115-20.
7. M. Kawaguchi, Y. Ohashi, and H. Tobushi: *JSME Int. J.*, 1991, vol. 34, pp. 76-82.
8. H. Tobushi, H. Iwanaga, K. Tanaka, T. Hori, and T. Sawada: *JSME Int. J.*, 1992, vol. 35, pp. 271-77.

9. N. Hagemeister, L.H. Yahia, C. Armand, and T. Lours: *1st Int. Conf. on Shape Memory and Superelastic Technologies*, Pacific Grove, CA, 1994, pp. 395-400.
10. B. Strnadel, S. Ohashi, H. Ohtsuka, S. Miyazaki, and T. Ishihara: *Mater. Sci. Eng. A*, 1995, vol. A203, pp. 187-96.
11. B. Strnadel, S. Ohashi, H. Ohtsuka, T. Ishihara, and S. Miyazaki: *Mater. Sci. Eng. A*, 1995, vol. A202, pp. 148-56.
12. R. Vaidyanathan, M.A.M. Bourke, and D.C. Dunand: *J. Appl. Phys.*, 1999, vol. 86, pp. 3020-29.
13. M.A.M. Bourke, R. Vaidyanathan, and D.C. Dunand: *Appl. Phys. Lett.*, 1996, vol. 69, pp. 2477-79.
14. Y.C. Shu and K. Bhattacharya: *Acta Mater.*, 1998, vol. 46, pp. 5457-73.
15. K. Gall, H. Sehitoglu, Y.I. Chumlyakov, and I.V. Kireeva: *Acta Mater.*, 1999, vol. 47, pp. 1203-17.
16. M.A.M. Bourke, J.A. Goldstone, and T.M. Holden: in *Measurement of Residual and Applied Stress Using Neutron Diffraction*, M.T. Hutchings and A.D. Krawitz, eds., Kluwer Academic, Dordrecht, Netherlands, 1992, pp. 369-82.
17. N. Shi, M.A.M. Bourke, J.A. Roberts, and J.E. Allison: *Metall. Mater. Trans. A*, 1997, vol. 28A, pp. 2741-53.
18. R. Vaidyanathan: Ph.D. Thesis, Massachusetts Institute of Technology, Cambridge, MA, 1999.
19. R. Vaidyanathan, M.A.M. Bourke, and D.C. Dunand: *Acta Mater.*, 1999, vol. 47, pp. 3353-66.
20. R. Vaidyanathan, M.A.M. Bourke, and D.C. Dunand: *Mater. Sci. Eng. A*, 1999, vols. A273–A275, pp. 404-09.
21. H.M. Rietveld: *J. Appl. Cryst.*, 1969, vol. 2, pp. 65-71.
22. A.C. Larson and R.B. VonDreele: Report No. LAUR 8-748, Los Alamos National Laboratory, Los Alamos, NM, 1986.
23. R.B. VonDreele: *J. Appl. Cryst.*, 1997, vol. 30, pp. 517-25.
24. H.J. Bunge: *Texture Analysis in Materials Science*, Butterworth-Heinemann, London, 1982.
25. K.L. Fukami-Ushiro and D.C. Dunand: *Metall. Mater. Trans. A*, 1996, vol. 27A, pp. 183-91.
26. E.F. Sturcken and J.W. Croach: *Trans. TMS-AIME*, 1963, vol. 227, pp. 934-40.
27. Y. Liu, I. Houver, H. Xiang, L. Bataillard, and S. Miyazaki: *Metall. Mater. Trans. A*, 1999, vol. 30A, pp. 1275-82.
28. T. Saburi and S. Nenno: in *Solid-Solid Phase Transformations*, H.I. Aaronson, ed., TMS-AIME, Warrendale, PA, 1981, pp. 1455-79.
29. D.C. Dunand, D. Mari, M.A.M. Bourke, and J.A. Roberts: *Metall. Mater. Trans. A*, 1996, vol. 27A, pp. 2820-36.
30. R. Plietsch and K. Ehrlich: *Acta Mater.*, 1997, vol. 45, pp. 2417-24.
31. M.R. Daymond, M.A.M. Bourke, and R.B.V. Dreele: *J. Appl. Phys.*, 1997, vol. 82, pp. 1554-62.
32. R. Vaidyanathan, U. Ramamurty, and D.C. Dunand: *Mater. Sci Eng. A*, 2000, vol. A289 (1–2), pp. 208-16.